

# Deciphering the Interactions of Bioactive Compounds in Selected Traditional Medicinal Plants Against Breast Cancer Via Machine Learning and Molecular Docking Approaches

Damilola S. Bodun <sup>1,\*</sup>, Olamide L. Onawola <sup>2</sup>, Dorcas T. Omonigbehin <sup>3</sup>,  
Damilola A. Omoboyowa <sup>1</sup>, Fatima Aminu <sup>1</sup>, Simbo T. Akinsulure <sup>1</sup>, Bolanle E. Adedapo <sup>1</sup>, Mary  
O. Alonge <sup>1</sup>, Precious A. Ajiboro <sup>1</sup>, Daniel O. Nwankwo <sup>1</sup>, Salimat Sofela <sup>4</sup>, Ibidun B. Isaac <sup>5</sup>

<sup>1</sup> Department of Biochemistry, Adekunle Ajasin University, Akungba-Akoko, Nigeria; dbodun56@gmail.com (D.S.B.); damilola.omoboyowa@aaau.edu.ng (D.A.O.); akinsuluresimbo@gmail.com (S.T.A); adedapobolanle99@gmail.com (B.E.A); maryalonge80@gmail.com (M.O.A); Fatimaaminu513@gmail.com (F.A.); danielogbonnayanwankwo@gmail.com (D.O.N.); preciousajiboro@gmail.com (P.A.A.);

<sup>2</sup> Molecular Biology Research Laboratory, Department of Microbiology, Covenant University, Nigeria; onawolydia2018@gmail.com;

<sup>3</sup> Department of Computer Science, Covenant University, Nigeria; omonigbehintemilade@gmail.com;

<sup>4</sup> Department of Chemistry, University of Lagos, Nigeria; salimatsofela@gmail.com;

<sup>5</sup> University of Missouri, St. Louis, U.S.A; ibidun07@gmail.com;

\* Correspondence: dbodun56@gmail.com;

Received: 30.05.2024; Accepted: 12.07.2025; Published: 7.09.2025

**Abstract:** Breast cancer is a severe disease that has a significant impact on numerous women worldwide, and is associated with the overexpression of EGFR, a critical enzyme involved in cancer progression. Although chemotherapy and targeted therapy have shown some success, the emergence of drug resistance, toxic side effects, and lack of efficacy in certain patients remain major challenges. As a result, there is an increasing desire to create novel therapeutic agents using natural sources that could potentially provide better effectiveness and fewer adverse effects. This study aims to investigate the potential anti-cancer properties of phytochemicals obtained from selected plants (*Ziziphus nummularia*, *Tinospora cordifolia*, *Momordica charantia*, *Cnidium monnieri*, and *Trigonella foenum graecum*) by checking their ability to inhibit EGFR. The study utilized a range of chemoinformatics and computational techniques, including virtual screening via Jupyter notebooks and the RDKit Library and structure-based screening (Rigid receptor docking, Induced fit docking, and Quantum polarized ligand docking) via the Maestro Schrödinger software, to identify potential compounds for breast cancer therapeutics. Subsequent analyses, such as DFT and AutoQSAR, were then employed to perform quantum calculations, compute descriptors, and predict the bioactivity of the identified top compounds. Among the screened compounds, five were found to have superior docking scores to the standard drug, Gefitinib. Further analysis using MMGBSA revealed that the lead compound, N-cis-Feruloyl tyramine, had a significantly better binding affinity to the target compared to the standard drug. ADMET predictions using the AdmetSAR server were then performed to evaluate the top-ranked compounds. Interestingly, the lead compound was found to be a P-gp substrate and not hepatotoxic, which is a significant advantage over Gefitinib. Quantum calculations show that the top compound, N-cis-Feruloyl tyramine, has a low ionization energy value, hence its strong interaction with our target protein. Although these results are encouraging, additional research is required to verify the efficiency and safety of the compounds discovered in this study through preclinical and clinical trials. Nevertheless, the use of computational methods to identify natural compounds for the treatment of breast cancer represents a hopeful approach to developing safe and effective therapies.

**Keywords:** molecular docking; EGFR; inhibitor; breast cancer; DFT.

© 2025 by the authors. This article is an open-access article distributed under the terms and conditions of the Creative Commons Attribution (CC BY) license (<https://creativecommons.org/licenses/by/4.0/>), which permits unrestricted use, distribution, and reproduction in any medium, provided the original work is properly cited. The authors retain copyright of their work, and no permission is required from the authors or the publisher to reuse or distribute this article, as long as proper attribution is given to the original source.

## 1. Introduction

Cancer is one of the main causes of mortality worldwide, and the number of cancer-related deaths is rising every day [1]. Breast cancer, which accounts for 6.6% of all cancer deaths worldwide, is the fifth most fatal disease [2]. It is the most common cancer in women globally. Yearly, about 25% of cancer patients are women who have been diagnosed with breast cancer worldwide [3]. EGFR is an abnormal epidermal growth factor receptor that characterizes most human cancers, including breast cancer [4]. There is usually an overexpression of EGFR in inflammatory breast cancer (IBC) and about half of triple-negative breast cancer cases (TNBC) [5]. Therefore, EGFR has been studied as an inhibitor of breast cancer treatments. EGFR is in the ErbB family, which has three other closely related members: ErbB-2 or HER2, ErbB-3 or HER3, and ErbB-4 or HER4. EGFR is also referred to as HER1 or ErbB-1. These epidermal growth factors are responsible for the proliferation of cancerous cells and the regulation of cells [6]. Today, several drugs have been developed for the inhibition of EGFR, such as erlotinib, afatinib, Gefitinib, and osimertinib. Even though they are known to cause short-term to long-term side effects, such as skin rash, dry skin, infection of the finger or toe, stomatitis, diarrhea, and appetite loss [7], some people, particularly in developing nations, find them to be fairly affordable. Thus, this particular study shows the effect of five different medicinal plants on breast cancer, which are also known to inhibit the EGFR to prevent cancer growth via an *in silico* approach. Fenugreek (*Trigonella foenum graecum*) is a medicinal plant with anticancer properties used by cancer patients, it is cultivated in North Africa and the Mediterranean region in India [8]. The extracts and compounds of Fenugreek were discovered to target at least five characteristics of cancer which include, proliferation, inflammation, angiogenesis, invasion, and metastasis [8]. Similarly, *Ziziphus nummularia* has been reported to have some antioxidant, anti-inflammatory, antimicrobial, antiproliferative, hypoglycemic, and hypolipidemic properties [9]. Likewise, quite a large number of phytochemicals have been segregated from various parts of the plant, such as tannins, flavonoids, steroids, glycosides, and alkaloids. Identified Compounds (IC) known as triterpene derivatives isolated from the root bark, exhibit a high level of cytotoxicity in numerous human cancer cell lines *in vitro*, which includes breast cancer, leukemia, ovarian cancer, and kidney carcinoma [9]. Another phytoconstituent isolated from the *Ziziphus nummularia* is Lapachol, which has been reported to have a very high level of antitumor activity. *Tinospora cordifolia* (Tc), universally known as “Guduchi,” has also been reported to possess anti-carcinogenic properties. The phytochemicals of ethanolic extract from *Tinospora cordifolia* have been reported to be effective in cell cytotoxicity, apoptosis induction, and cell cycle arrest in the G2/M phase of human breast cancer cell lines [10]. Another phytocomponent of Tc is phenolic contents (quercetin and rutin) exhibiting anti-proliferative activity on human breast cancer [10]. Prevention of breast cancer through diet is another approach to controlling breast cancer. Therefore, it does this by employing dietary chemopreventive substances to induce cell cycle arrest or apoptosis, which kills genetically altered, premalignant, and malignant cells, and inhibits the growth and development of carcinogenesis [11]. A nutrient-rich medicinal plant

called bitter melon or bitter gourd (*Momordica charantia*) is grown in several countries' tropical and subtropical climates. It has a long history of usage as a natural remedy and is filled with bioactive substances, such as triterpenoids, triterpene glycosides, phenolic acids, flavonoids, lectins, sterols, and proteins, that may have anticancer properties without causing any discernible side effects [12]. Breast cancer cells MCF-7 and MDA-MB-231 experienced growth inhibition and apoptosis when exposed to the water extracted from bitter melon fruit [12]. The dry fruit of the Umbelliferae plant *Cnidium monnieri* (L.) contains 364 components, the majority of which are coumarins like osthole, imperatorin, bergapten, isopimpinellin, xanthotoxin, cnidimonal, and glucosides [13]. Recent research has demonstrated the anticancer properties of osthole, an active component extracted from the fruit of *Cnidium monnieri* (L.) [14]. *In vitro* experiments revealed that osthole (20 g/mL) inhibited human breast cancer in a dose- and time-dependent manner. Furthermore, it has been demonstrated to inhibit tumor-angiogenic factors such as vascular endothelial growth factor (VEGF) and MMP-9. Moreover, it might inhibit the activity of HER-2/neu-positive breast cancer cells, which would impede the downstream of the MAPK signaling pathway [13]. As a result, this research aims to examine how the bioactive chemicals in fenugreek (*Trigonella foenum graecum*), *Ziziphus nummularia*, *Tinospora cordifolia*, bitter melon (*Momordica charantia*), and *Cnidium monnieri* (L.) Cusson interact as inhibitors against breast malignancy.

## 2. Materials and Methods

### 2.1. Target preparation.

The protein structure of the Epidermal Growth Factor Receptor (EGFR) in complex with an allosteric inhibitor (PDB ID – 5D41) was obtained from the RCSB protein Data Bank (<http://www.rcsb.org/pdb>) [15]. To prepare the structure for further analysis, it was imported into Maestro and underwent pre-processing steps including the addition of bond orders, hydrogen atoms, and loop filling, while removing water molecules [16]. Automated and interactive optimization was utilized to optimize hydrogen bond assignment and refine the structure, resulting in a minimized RMSD value. Finally, the OPLS 2005 force field was used to determine partial atomic charges [17].

### 2.2. Filtering by Lipinski and pains.

Phytochemicals present in five plants were identified through a literature search of various sources [18-22]. In total, 413 ligands were obtained from the PubChem website (<https://pubchem.ncbi.nlm.nih.gov/>). The phytochemicals' names and SMILES strings were compiled in an Excel sheet and subsequently imported into a Jupyter notebook using the Pandas library. The compounds were then filtered based on compliance with Lipinski's rule and the presence of PAINs (Pan Assay Interference Compounds). The resulting list of filtered compounds was saved as a CSV file and subsequently converted back into the SDF format using DataWarrior software.

### 2.3. Ligand preparation.

To prepare the ligand structures, the ADMET and PAINs filtered compounds were used and processed using LigPrep, a module of the Maestro Schrodinger, which was designed to generate high-quality 3D structures for a large number of drug-like molecules [23, 24].

#### 2.4. Grid generation.

The active site of EGFR was characterized by determining its binding orientation and size using the receptor grid generation module in Schrödinger Maestro software. The coordinates for scoring were calculated based on the co-crystallized ligand that was present within the EGFR binding pocket. The x, y, and z grid coordinates were measured to be -23.67, 31.37, and 12.23, respectively.

#### 2.5. Rigid receptor docking or conventional docking.

In molecular docking studies, rigid receptor docking is a technique used to investigate the interaction between a target receptor and a small molecule ligand. The receptor is kept in a fixed or "rigid" conformation during the docking simulation, while the ligand is free to move and rotate within the receptor's binding site [25-27]. In this study, all 218 filtered ligands were initially docked using the HTVS docking protocol, and a docking score threshold of -5.0 kcal/mol was used to filter the compounds down to 96. These 96 compounds were subsequently docked again using the Standard Precision (SP) technique and were filtered again using a docking score threshold of -7.0 kcal/mol, which resulted in 20 compounds that were finally docked using the Extra Precision (XP) model.

#### 2.6. Estimation of binding energy.

Good poses and high scores for the docked complexes were correlated in this study, according to the XP docking results. However, the free binding energy was determined using the Prime module of Maestro's Molecular Mechanics Generalized Born Surface Area (MM-GBSA) approach to assess the probable biological response of these complexes [28, 29]. For this analysis, the top five compounds, including the standard drug, were chosen. Using the VSGB 2.0 implicit solvation model and OPLS-2005 force field, the MM-GBSA computational technique assesses the binding free energy (binding affinity) and minimizes the docked protein-ligand complex. The binding free energy was calculated using the following equation:

$$\Delta G^{\text{bind}} = G^{\text{complex}} - (G^{\text{protein}} + G^{\text{Ligand}}) \quad (1)$$

where  $\Delta G^{\text{bind}}$  is the protein-ligand complex's binding free energy,  $G^{\text{complex}}$  is the complex's free energy, and  $G^{\text{protein}}$  and  $G^{\text{Ligand}}$ , respectively, are the free energies of the protein and the ligand.

#### 2.7. Induced fit docking (IFD).

During this docking simulation, the residues in the EGFR-binding site were viewed as flexible. All parameters were left at their default settings, and the Schrödinger induced-fit docking module was employed. The protein's active site residues were initially maintained stiffly while the ligands were docked into the protein using the Glide protocol (SP), and the top twenty poses were retained (i.e., Standard Protocol). The Prime refinement module was then used to further improve the protein side chains or backbone. The protein-ligand complex was then ranked using the induced fit docking score after the ligand was redocked into the improved protein conformation.

### 2.8. QPLD docking.

The QPLD method uses QSite v6.1 and Jaguar v8.2 to properly compute the charges of the ligand and the interacting active site residues using a hybrid QM/MM approach [17]. The polarization of charges on the lead by the receptor is another factor considered by QPLD. Glide SP mode was first utilized to determine the top five poses for each lead. To determine the partial atomic charges of the bound ligands in each position, ab initio methods were used. Pose rejection criteria included RMSD and maximum atomic displacement thresholds of 0.5 and 1.3, respectively. The leads were then re-docked with Glide XP using the charge settings that had been previously computed in Q-site refining. The E-model score was used to grade the poses. Only the lead compound and standard were used for this technique.

### 2.9. Development of auto-qsar model.

To obtain data on the activity of EGFR inhibitors, 35 inhibitors were extracted from the ChEMBL database using the protein's FASTA sequence obtained from the PDB as a query. The extracted compounds were converted into a ".SDF" format using Datawarrior software. With the use of the AutoQsar module, a QSAR model was created using these compounds. The best-performing model, KPLS\_MOLPRINT2D\_45, was selected based on its rank.

### 2.10. Density functional theory analysis.

Density functional theory (DFT) analysis was used to calculate the molecular electrostatic properties of the top five compounds for further research. Initially, a search for conformer distribution was carried out for each of the leading compounds, and the most stable conformer was chosen for a comprehensive DFT calculation using the B3LYP functional method and a 6-31G\* basis set. Several parameters, including lowest unoccupied molecular orbital (LUMO) energy and highest occupied molecular orbital (HOMO) energy, were estimated for this purpose using the Spartan 10 software. Using these parameters, the following equations were used to determine various parameters, including energy gap (Eg), ionization energy (I), electron affinity (A), chemical hardness ( $\eta$ ), chemical softness ( $\delta$ ), and electronegativity ( $\chi$ ):

The energy bandgap (Eg) was calculated from the difference between ELUMO and EHOMO.

$$E_g = E_{LUMO} - E_{HOMO} \quad (2)$$

Electron affinity (A) and ionization potential (I) are related to ELUMO and EHOMO using Koopman's theorem [30].

$$I = -E_{HOMO} \quad (3)$$

$$A = -E_{LUMO} \quad (4)$$

The electronegativity ( $\chi$ ) and chemical hardness ( $\eta$ ) of the compounds were calculated using Parr and Pearson [31].

$$\chi = \frac{I+A}{2} \quad (5)$$

$$\eta = \frac{I-A}{2} \quad (6)$$

Chemical softness ( $\delta$ ) is the inverse of chemical hardness

$$\delta = \frac{1}{\eta} \quad (7)$$

### 2.11. ADME prediction.

The ADME characteristics (Absorption, Distribution, Metabolism, and Excretion) of the top five compounds, including the standard drug, were examined using the admetSAR server (<http://lmmd.ecust.edu.cn/admetSAR2/>) to predict their efficacy. These properties are crucial in drug development and help determine the likelihood of a compound becoming an effective drug.

## 3. Results and Discussion

### 3.1. Lipinski and PAINS filtering.

Lipinski's "rule of 5" is a widely known virtual screening method that was initially used to filter out compounds that are unlikely to be bioavailable [32]. This rule was used to exclude any compound that violated the rule from the initial screening process. This approach helped to optimize the screening process by filtering out compounds that are unlikely to be successful drug candidates.

However, some substructures, referred to as Pan-Assay Interference Compounds (PAINS), have been found to regularly produce false positive results in biochemical assays, resulting in the loss of time, resources, and money in the drug discovery process [33]. Instead of particularly affecting one desired target, PAINS typically interact non-specifically with a variety of biological targets. A typical academic screening library contains between 5 and 12 percent of all compounds that are PAINS, many of which share disruptive functional groups[34].

To avoid false positives and prevent the optimization of compounds that are unlikely to be successful drug candidates, compounds that contain PAINS substructures were filtered out using the PAINS implemented in the RDKit library (Supplementary Figure 1). This strategy helps to optimize the screening process by filtering out compounds that are unlikely to be "true" hits and avoiding wasted time and resources on optimizing these compounds.

### 3.2. Rigid receptor docking (RRD) and MMGBSA.

The binding affinities of five molecules were compared to that of Gefitinib, a reference drug, in this molecular docking simulation. The findings demonstrated that, with scores ranging from -8.617 kcal/mol to -8.096 kcal/mol, all five molecules exhibited better binding affinity than Gefitinib (Table 1). N-cis-Feruloyl Tyramine, which came in first place, formed three hydrogen bonds with the target through the amino acids MET 793, ASP 855, and PHE 856. It also had the highest score of -8.617 kcal/mol (Table 2, Figure 1).

**Table 1.** Docking scores (RRD, IFD, and QPLD) of the top-scoring compounds and standard against EGFR.

Title	Docking score	MMGBSA dG Bind	IFD docking score	IFD score	QPLD docking score	QPLD eModel
N-cis-Feruloyl tyramine	-8.617	-62.68	-9.617	-642.22	-8.612	-81.186
kaempferol	-8.419	-41.5				
naringenin	-8.352	-41.01				
Allylphenoxycetate	-8.222	-37.43				
Diosmetin	-8.096	-36.81				
Gefitinib (Standard)	-5.537	-44.59	-10.052	-643.79	-7.287	-89.808

**Table 2.** Interaction profile of top-ranked compounds, including the standard within the active site of EGFR.

Title	H-Bond	Hydrophobic amino acids	Other interactions
N-cis-Feruloyl tyramine	MET 793, ASP 855, PHE 856	LEU 718, VAL 726, ALA 743, MET 766, CYS 775, LEU 777, LEU 844, LEU 788, MET 790, LEU 792, MET 793, CYS 797, PHE 856, LEU 858	NONE
Kaempferol	LYS 745, GLU 762, CYS 775, ASP 855	PHE 723, LEU 747, ILE 759, ALA 763, MET 766, LEU 788, MET 790, CYS 775, LEU 777, PHE 856, LEU 858	NONE
Naringenin	CYS 775, GLU 762	PHE 723, LEU 747, ILE 759, ALA 763, MET 766, LEU 788, MET 790, CYS 775, LEU 777, PHE 856, LEU 858	NONE
Allylphenoxyacetate	ASP 855	LEU 747, ALA 763, MET 766, LEU 777, CYS 775, PHE 856, LEU 858, LEU 788, MET 790, ILE 759, PHE 723	NONE
Diosmetin	LYS 745, GLU 762	LEU 747, PHE 723, LEU 788, MET 790, CYS 775, LEU 777, PHE 856, MET 766, LEU 858, ILE 759	NONE
Gefitinib	NONE	PHE 723, LEU 747, LEU 788, MET 790, LEU 777, PHE 856, LEU 858, MET 766, ALA 763, ILE 759	HALOGEN BOND: PHE 856

Additionally, LEU 718, VAL 726, ALA 743, MET 766, CYS 775, LEU 777, LEU 844, MET 790, LEU 792, CYS 797, PHE 856, and LEU 858 formed hydrophobic contacts with N-cis-Feruloyl tyramine in the target's active site.

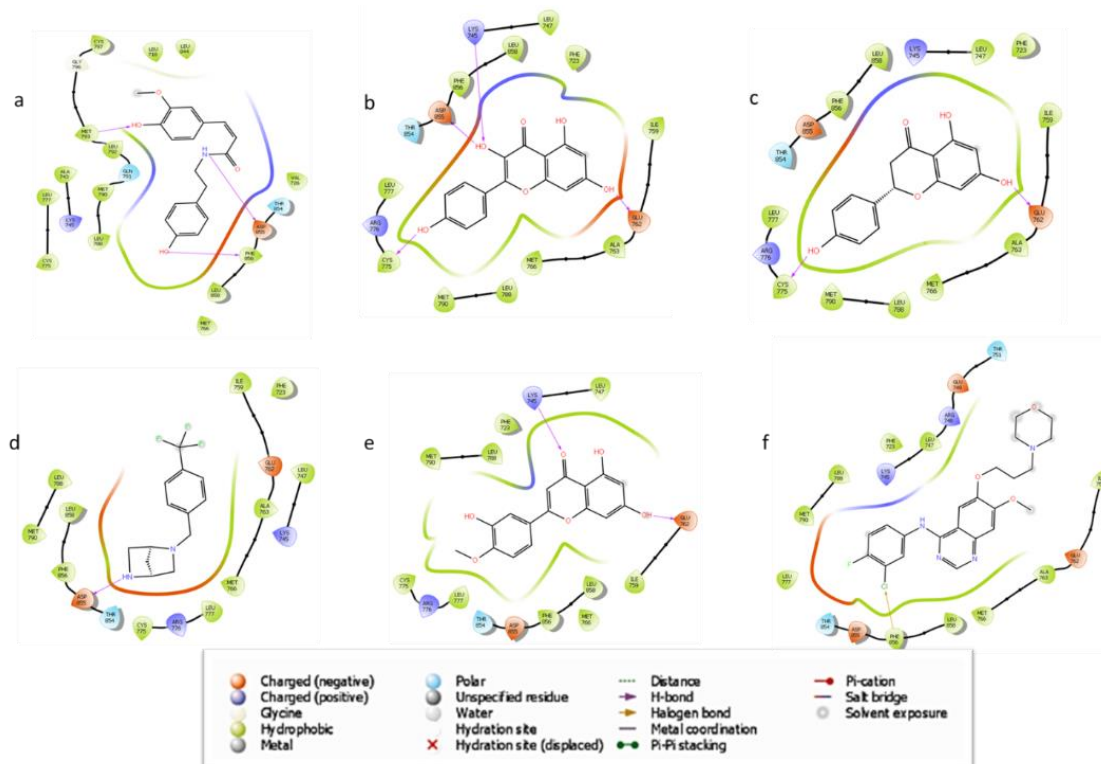


**Figure 1.** 2D interacting plots between (a) N-cis-Feruloyl tyramine; (b) Kaempferol; (c) Naringenin; (d) Allylphenoxyacetate; (e) Diosmetin; (f) Gefitinib (Standard) with residues at the binding pocket of EGFR

The second-ranked compound, Kaempferol, had a score of -8.352 kcal/mol and formed four hydrogen bonds with LYS 745, GLU 762, CYS 775, and ASP 855 amino acids. It also made significant hydrophobic interactions with PHE 723, LEU 747, ILE 759, ALA 763, MET 766, LEU 788, MET 790, CYS 775, LEU 777, PHE 856, and LEU 858. Naringenin, with a score of -8.352 kcal/mol, formed two hydrogen bond interactions with CYS 775 and GLU 762,

and made hydrophobic interactions with PHE 723, LEU 747, ILE 759, ALA 763, MET 766, LEU 788, MET 790, CYS 775, LEU 777, PHE 856, and LEU 858.

Allylphenoxyacetate, with a score of -8.222 kcal/mol, formed one hydrogen bond interaction with ASP 855 and interacted hydrophobically with LEU 747, ALA 763, MET 766, LEU 777, CYS 775, PHE 856, LEU 858, LEU 788, MET 790, ILE 759, and PHE 723. Diosmetin, with a score of -8.096 kcal/mol, formed two hydrogen bond interactions with LYS 745 and GLU 762, and made hydrophobic interactions with LEU 747, PHE 723, LEU 788, MET 790, CYS 775, LEU 777, PHE 856, MET 766, LEU 858, and ILE 759.

Interestingly, Gefitinib did not form any hydrogen bond interactions but instead formed a halogen bond with PHE 856. It also interacted hydrophobically with several amino acids in the active site, including PHE 723, LEU 747, LEU 788, MET 790, LEU 777, PHE 856, LEU 858, MET 766, ALA 763, and ILE 759.

The complexes were submitted to MM-GBSA post-docking analysis to validate the results from the docking technique. The stability of the complexes generated following the docking simulation is evaluated using this approach, which calculates the binding free energy of the ligand with the receptor [35]. The standard drug came up second with an MM-GBSA score of -44.59, while the hit compound had the best score of -62.68 (Table 1).

### 3.3. Induced fit docking.

Induced fit docking (IFD) and rigid receptor docking (RRD) are both popular methods for predicting how ligands will bind to protein targets. The difference between the two methods lies in the flexibility of the protein receptor during the docking process. RRD assumes the protein receptor is rigid and can miss important binding interactions that require flexibility, resulting in less accurate predictions. IFD, on the other hand, accounts for the flexibility of both the ligand and the receptor, leading to more accurate predictions, especially for flexible receptors and ligands [36].

In this study, due to computational limitations, only the lead ligand and a standard drug were subjected to IFD. The results of IFD showed that the standard drug, Gefitinib, had a more favorable docking score and IFD score (-10.052 kcal/mol and -643.79) than the lead ligand (Table 1). This was interesting because the standard drug lost a halogen bond with PHE 866 during conventional docking, but gained a PI-PI stacking interaction with the same amino acid and formed a new H-bond with ASP 855 during IFD (Table 3).

**Table 3.** Interaction profile of lead compound and standard drug within the active site of EGFR after IFD.

Title	H-Bond	Other interactions
N-cis-Feruloyl tyramine	MET 793, ASP 855 (2), PHE 856, GLN 791	NONE
Gefitinib	ASP 855	NONE

The lead ligand had a better docking score using IFD (-9.617 kcal/mol) but was lower than the standard drug. Furthermore, the lead ligand gained two extra H-bonds, one with GLN 791 and the other with ASP 855, during IFD (Figure 2).

These results demonstrate the importance of H-bond additions in the binding of Gefitinib to EGFR. Therefore, we noted how IFD can improve the accuracy and reliability of docking predictions, especially for flexible receptors and ligands, and provide insight into the mechanism of binding and structural changes in the receptor upon ligand binding.

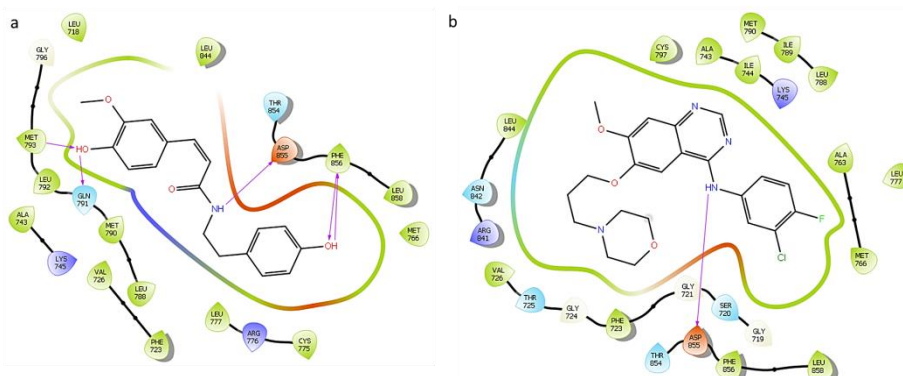


**Figure 2.** 2D interacting plots between (a) N-cis-Feruloyl tyramine; (b) Gefitinib (Standard) with residues at the binding pocket of EGFR after Induced Fit Docking.

### 3.4. Quantum mechanics polarized ligand docking (QPLD).

In comparison to RRD and IFD, QPLD involves the polarization of the ligand by the protein's electric field, resulting in changes to the ligand's electron density distribution and energy [37]. This technique uses QM calculations to model these changes and estimate the binding energy of the ligand to the protein. QPLD is particularly useful for predicting the binding mode of ligands with a large number of polar functional groups that may not be accurately modeled by other methods. However, due to computational limitations, QPLD was only performed on the lead and standard ligands.

Interestingly, the lead ligand achieved a better docking score (-8.612 kcal/mol) than the standard drug (-7.287kcal/mol) when using QPLD (Table 1). Upon examining the interactions between the compounds and protein, we observed the loss of two 2-bonds, including the popular H-bond with PHE 856, and the formation of a new H-bond with CYS 775 in the lead ligand (Table 4). In contrast, Gefitinib lost its H-bond with ASP 855 during IFD and transferred it to ASH 837, then reformed the lost halogen bond with PHE 856 during IFD, but with another amino acid, LYS 745 (Figure 3). The weakness of the halogen bond is evident in the reduction of the docking scores.

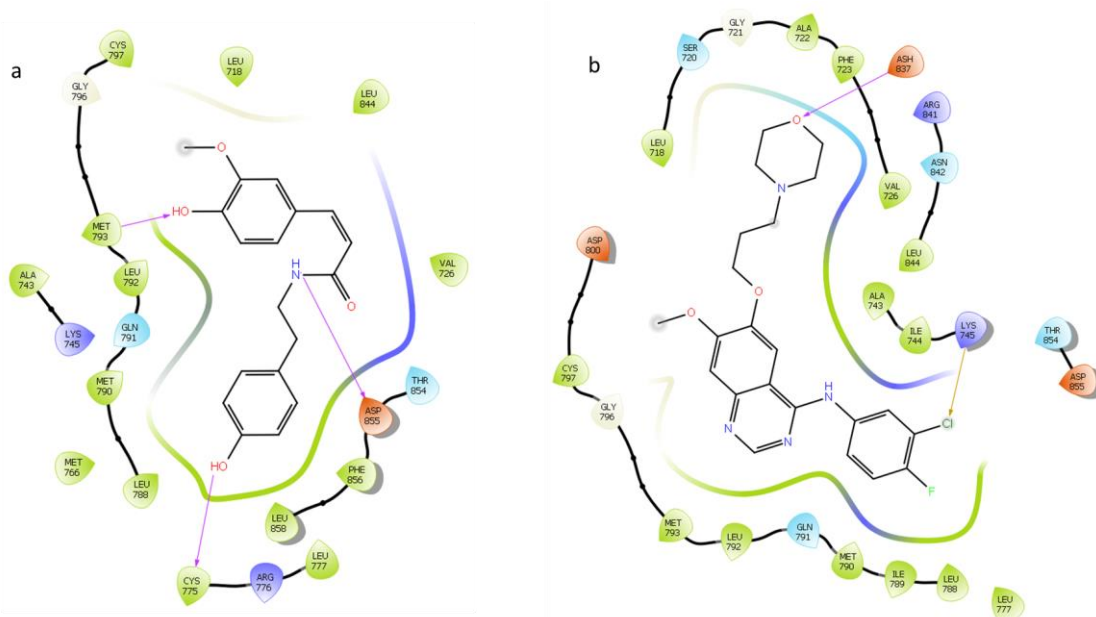


**Table 4.** Interaction profile of lead compound and standard drug within the active site of EGFR after QPLD.

Title	H-Bond	Other interactions
N-cis-Feruloyl tyramine	MET 793, CYS 775, ASP 855	NONE
Gefitinib	ASH 837	HALOGEN BOND: LYS 745

However, the Emodel score, which measures the energy required to form and maintain the complex between the ligand and the protein, considering factors such as van der Waals interactions, electrostatic interactions, and hydrogen bonding, shows that the standard drug (-89.808) requires slightly more energy to maintain the complex with the protein than the lead ligand (-81.186).

### 3.5. Density functional theory analysis.

The electronic properties of a compound are important determinants of its chemical reactivity and kinetic stability. The HOMO and LUMO parameters, which respectively signify the electron donation and acceptance of a molecule, play a crucial role in determining its electron-donating and accepting ability [16]. The distribution of these around the structure of the molecules is depicted in Supplementary Table 3.

Another important electronic parameter is the energy band gap ( $E_g$ ), which is dependent on the HOMO-LUMO difference. This parameter is a critical determinant of the chemical reactivity and kinetic stability of a compound. A larger energy band gap signifies lower reactivity but higher stability, and vice versa.

Among the natural compounds considered, Allylphenoxyacetate exhibits the highest kinetic stability but the lowest reactivity, as seen from the energy band gap values in the order: Kaempferol < Diosmetin < N-cis-Feruloyl tyramine < naringenin < Allylphenoxyacetate (Table 5). The ionization energy (I) is another electronic parameter that measures the energy required to remove an electron from a molecule. Compounds with lower ionization energy values indicate higher reactivity and lower chemical inertness. N-cis-Feruloyl tyramine, with one of the lowest ionization energy values, had the best interaction with our target protein. Naringenin has the highest ionization energy, implying higher stability and chemical inertness.

**Table 5.** DFT calculations of the electronic behavior of the hit compounds.

Compounds	$E_{\text{HOMO}}$ (eV)	$E_{\text{LUMO}}$ (eV)	$E_g$ (eV)	I (eV)	A (eV)	$\eta$ (eV)	$\delta$ (eV <sup>-1</sup> )	$\chi$ (eV)
N-cis-Feruloyl tyramine	-5.77	-1.24	4.53	5.77	1.24	2.265	0.441501	3.505
kaempferol	-5.53	-1.81	3.72	5.53	1.81	1.86	0.537634	3.67
naringenin	-6.04	-1.43	4.61	6.04	1.43	2.305	0.433839	3.735
Allylphenoxyacetate	-5.55	-0.69	4.86	5.55	0.69	2.43	0.411523	3.12
Diosmetin	-5.84	-1.68	4.16	5.84	1.68	2.08	0.480769	3.76

Furthermore, electron affinity (A) measures the energy released upon adding an electron to a neutral molecule, with compounds exhibiting high electron affinity being more reactive [38]. Among the compounds considered, Kaempferol displays the highest reactivity, with an electron affinity of 1.81 eV.

Chemical hardness refers to a molecule's ability to resist receiving or donating electrons, affecting its water solubility, whereas softness indicates a molecule's propensity for easy electron donation or acceptance, which is relevant to its reactivity with biological targets [39]. The chemical hardness and softness of a molecule are significant factors in its stability and reactivity in addition to the energy band gap. Hard molecules have a larger energy band gap, while soft molecules have a smaller gap [16]. The order of chemical hardness among the natural compounds considered is Allylphenoxyacetate > naringenin > N-cis-Feruloyl tyramine

> Diosmetin > kaempferol (Table 5). Furthermore, Diosmetin exhibits a greater electronegativity, indicating its strong ability to attract electrons.

### 3.6. Auto QSAR.

The AutoQSAR module maintains the same distribution pattern in the learning set while using a randomized approach to choose training and test sets in a ratio of 75% and 25%, respectively (Supplementary Table 1). Using the Canvas module, it generates 2D fingerprints (dendritic, linear, MOLPRINT2D, or radial) and 497 physicochemical and topological descriptors. Predictive models are then developed using a variety of machine learning techniques (Bayes, KPLS, MLR, PCR, PLS, and RP), with only Bayes and KPLS using both descriptors and fingerprints [40].

The module ranks the models according to their merits after assessing each model's accuracy with the training and test sets using a robust score function. With a Standard Deviation (S.D.) of 0.6388, a Coefficient of Determination (R<sup>2</sup>) of 0.8395, a Root Mean Squared Error (RMSE) of 0.6314, and a Cross-Validation (Q<sup>2</sup>) of 0.8094, Kpls molprint2D 45 was the top QSAR model (Supplementary Table 2). The scatter plot of the QSAR model is shown in Figure 4.

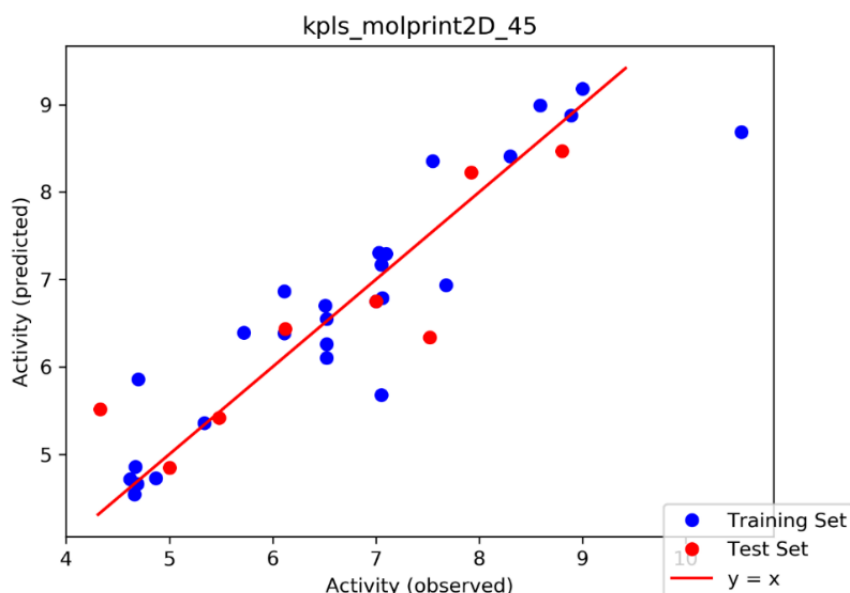


**Figure 4.** Scatter plot for the best AutoQSAR model (kpls\_molprint2D\_45) for EGFR.

The standard drug had a higher  $pIC_{50}$  value than the hits, as shown in Table 6, when the QSAR model was applied to compare the  $pIC_{50}$  values of the hits with the standard drug.

**Table 6.** Predicted bioactivity of the lead compounds and standard against EGFR by QSAR model.

Title	Pred $pIC_{50}$
N-cis-Feruloyl tyramine	5.046
kaempferol	5.724
naringenin	5.417
Allylphenoxyacetate	5.841
Diosmetin	5.82
Gefitinib	7.553

### 3.7. Pharmacokinetics.

The ADMET predictions were used to evaluate the potential of drug molecules in biological systems based on their pharmacological and pharmacodynamic properties.

Pharmacokinetic tests were conducted on all hit molecules, and penetrability studies were performed using the Caco-2 cell line to determine the intestinal digestion potential of the drug molecules. Caco-2 permeability was observed in Naringenin, Allylphenoxyacetate, and Diosmetin, while the lead compound and standard drug did not show this property. Only the lead compound was predicted to be a P-gp substrate, while only the standard drug was predicted to be a P-gp inhibitor (Figure 5). P-glycoprotein (P-gp) is an essential component of drug transport. All ligands were found to be HIA positive, indicating that they would be absorbed by the intestine. However, only Allylphenoxyacetate and the standard drug did not exhibit the potential to cross the BBB, reducing the likelihood of adverse effects in the sensory system. The lead ligand and Allylphenoxyacetate were not predicted to be CYP1A2 inhibitors, but all other hits were. Moreover, only Allylphenoxyacetate was predicted to be a non-inhibitor for CYP3A4, while all hits except Naringenin displayed substrate properties for this enzyme (Figure 5). None of the compounds, except for Kaempferol, were found to be carcinogenic or mutagenic. In conclusion, the lead compound, N-cis-Feruloyl tyramine, demonstrated outstanding performance in several areas of the study compared to the positive controls.



**Figure 5.** ADMET properties of the lead compounds and the standard.

The lead compound from this study, n-cis feruloyl tyramine, has been reported for oncogenic effects. In a study, at 0.8 mg-L<sup>-1</sup>, it led to 10.20% growth inhibition and 31.6% chemotaxis inhibition in MDA-MB-231 cells. With an increased concentration of 4 mg-L<sup>-1</sup>, the rates rose to 12.33% and 37.9%, respectively, indicating a dose-dependent impact on cell growth and chemotaxis [41]. N-cis-feruloyl-tyramine has demonstrated the ability to inhibit mushroom tyrosinase activity, making it a potential treatment for hyperpigmentation [42]. Additionally, the anti-cancer properties of Kaempferol, one of the hit compounds, have been

attributed to its inhibition of EGFR-related Src, ERK1/2, and AKT pathways, which shows its potential for treating pancreatic cancer [43].

#### **4. Conclusions**

This study highlights the necessity for additional computational studies following the standard docking process. Although the lead compound exhibits a close and higher binding affinity to the target protein compared to the standard drug in both Induced Fit Docking and Quantum-Mechanical Polarized Docking, respectively, further computational and experimental investigations are necessary to validate the effectiveness of the top ligand and other hits as potential breast cancer drugs by inhibiting EGFR.

#### **Author Contributions**

Conceptualization, D.S.B, O.L.O, D.T.O and S.S.; methodology, D.S.B, M.O.A.; software, B.E.A.; validation, S.T.A., I.B.I., and D.A.O.; formal analysis, D.S.B.; investigation, P.A.A.; resources, O.L.O.; data curation, D.O.N.; writing—original draft preparation, D.T.O.; writing—review and editing, F.A, M.O.A.; visualization, B.E.A.; supervision, D.S.B, D.A.O.; project administration, S.T.A.; All authors have read and agreed to the published version of the manuscript.

#### **Institutional Review Board Statement**

Not applicable.

#### **Informed Consent Statement**

Not applicable.

#### **Data Availability Statement**

Data supporting the findings of this study are available upon reasonable request from the corresponding author.

#### **Funding**

This research received no external funding.

#### **Acknowledgments**

None.

#### **Conflicts of Interest**

The authors declare no conflict of interest.

#### **References**

1. Ohiagu, F.O.; Chikezie, P.C.; Chikezie, C.M.; Enyoh, C.E. Anticancer activity of Nigerian medicinal plants: a review. *Future J. Pharm. Sci.* **2021**, *7*, 70, <https://doi.org/10.1186/s43094-021-00222-6>.

2. Huang, J.; Chan, P.S.F.; Lok, V.; Chen, X.; Ding, H.; Jin, Y.; Yuan, J.; Lao, X.-q.; Zheng, Z.-J.; Wong, M.C.S. Global incidence and mortality of breast cancer: a trend analysis. *Aging (Albany NY)* **2021**, *13*, 5748-5803, <https://doi.org/10.18632/aging.202502>.
3. Sun, S.; Zhao, Z.; Yang, N.; Xu, F.; Lu, J.; Zhu, Y.; Shi, W.; Jiang, J.; Yao, P.; Zhu, P. Risk Factors and Preventions of Breast Cancer. *International Journal of Biological Sciences*. **2017** *13(11)*, 1387. <https://doi.org/10.7150/ijbs.21635>
4. Ali, R.; Wendt, M.K. The paradoxical functions of EGFR during breast cancer progression. *Signal Transduct. Target. Ther.* **2017**, *2*, 16042, <https://doi.org/10.1038/sigtrans.2016.42>.
5. Masuda, H.; Zhang, D.; Bartholomeusz, C.; Doihara, H.; Hortobagyi, G.N.; Ueno, N.T. Role of epidermal growth factor receptor in breast cancer. *Breast Cancer Res. Treat.* **2012**, *136*, 331-345, <https://doi.org/10.1007/s10549-012-2289-9>.
6. Hsu, P.-C.; Jablons, D.M.; Yang, C.-T.; You, L. Epidermal Growth Factor Receptor (EGFR) Pathway, Yes-Associated Protein (YAP) and the Regulation of Programmed Death-Ligand 1 (PD-L1) in Non-Small Cell Lung Cancer (NSCLC). *Int. J. Mol. Sci.* **2019**, *20*, 3821, <https://doi.org/10.3390/ijms20153821>.
7. Sharma, B.; Singh, V.J.; Chawla, P.A. Epidermal growth factor receptor inhibitors as potential anticancer agents: An update of recent progress. *Bioorg. Chem.* **2021**, *116*, 105393, <https://doi.org/10.1016/j.bioorg.2021.105393>.
8. El Bairi, K.; Ouzir, M.; Agnieszka, N.; Khalki, L. Anticancer potential of *Trigonella foenum graecum*: Cellular and molecular targets. *Biomed. Pharmacother.* **2017**, *90*, 479-491, <https://doi.org/10.1016/j.biopha.2017.03.071>.
9. Mesmar, J.; Abdallah, R.; Badran, A.; Maresca, M.; Shaito, A.; Baydoun, E. *Ziziphus nummularia*: A Comprehensive Review of Its Phytochemical Constituents and Pharmacological Properties. *Molecules* **2022**, *27*, 4240, <https://doi.org/10.3390/molecules27134240>.
10. Deepa, B.; Babaji, H.V.; Hosmani, J.V.; Alamir, A.W.H.; Mushtaq, S.; Raj, A.T.; Patil, S. Effect of *Tinospora cordifolia*-Derived Phytochemicals on Cancer: A Systematic Review. *Appl. Sci.* **2019**, *9*, 5147, <https://doi.org/10.3390/app9235147>.
11. Ray, R.B.; Raychoudhuri, A.; Steele, R.; Nerurkar, P. Bitter Melon (*Momordica charantia*) Extract Inhibits Breast Cancer Cell Proliferation by Modulating Cell Cycle Regulatory Genes and Promotes Apoptosis. *Cancer Res.* **2010**, *70*, 1925-1931, <https://doi.org/10.1158/0008-5472.CAN-09-3438>.
12. Sur, S.; Ray, R.B. Bitter Melon (*Momordica Charantia*), a Nutraceutical Approach for Cancer Prevention and Therapy. *Cancers* **2020**, *12*, 2064, <https://doi.org/10.3390/cancers12082064>.
13. Sun, Y.; Yang, A.W.H.; Lenon, G.B. Phytochemistry, Ethnopharmacology, Pharmacokinetics and Toxicology of *Cnidium monnieri* (L.) Cusson. *Int. J. Mol. Sci.* **2020**, *21*, 1006, <https://doi.org/10.3390/ijms21031006>.
14. Wang, L.; Peng, Y.; Shi, K.; Wang, H.; Lu, J.; Li, Y.; Ma, C. Osthole inhibits proliferation of human breast cancer cells by inducing cell cycle arrest and apoptosis. *J. Biomed. Res.* **2012**, *29*, 132-138, <https://doi.org/10.7555%2FJBR.27.20120115>.
15. Jia, Y.; Yun, C.-H.; Park, E.; Ercan, D.; Manuia, M.; Juarez, J.; Xu, C.; Rhee, K.; Chen, T.; Zhang, H.; Palakurthi, S.; Jang, J.; Lelais, G.; DiDonato, M.; Bursulaya, B.; Michellys, P.-Y.; Epple, R.; Marsilje, T.H.; McNeill, M.; Lu, W.; Harris, J.; Bender, S.; Wong, K.-K.; Jänne, P.A.; Eck, M.J. Overcoming EGFR(T790M) and EGFR(C797S) resistance with mutant-selective allosteric inhibitors. *Nature* **2016**, *534*, 129-132, <https://doi.org/10.1038/nature17960>.
16. Omoboyowa, D.A.; Iqbal, M.N.; Balogun, T.A.; Bodun, D.S.; Fatoki, J.O.; Oyeneyin, O.E. Inhibitory potential of phytochemicals from *Chromolaena odorata* L. against apoptosis signal-regulatory kinase 1: A computational model against colorectal cancer. *Comput. Toxicol.* **2022**, *23*, 100235, <https://doi.org/10.1016/j.comtox.2022.100235>.
17. Bodun, D.S.; Omoboyowa, D.A.; Omotuyi, O.I.; Olugbogi, E.A.; Balogun, T.A.; Ezeh, C.J.; Omirin, E.S. QSAR-based virtual screening of traditional Chinese medicine for the identification of mitotic kinesin Eg5 inhibitors. *Comput. Biol. Chem.* **2023**, *104*, 107865, <https://doi.org/10.1016/j.compbiolchem.2023.107865>.
18. Wani, S.A.; Kumar, P. Fenugreek: A review on its nutraceutical properties and utilization in various food products. *J. Saudi Soc. Agric. Sci.* **2018**, *17*, 97-106, <https://doi.org/10.1016/j.jssas.2016.01.007>.
19. El Maaiden, E.; El Kharrassi, Y.; Qarah, N.A.S.; Essamadi, A.K.; Moustaid, K.; Nasser, B. Genus *Ziziphus*: A comprehensive review on ethnopharmacological, phytochemical and pharmacological properties. *J. Ethnopharmacol.* **2020**, *259*, 112950, <https://doi.org/10.1016/j.jep.2020.112950>.

20. Tiwari, P.; Nayak, P.; Prusty, S.K.; Sahu, P.K. Phytochemistry and pharmacology of *Tinospora cordifolia*: A review. *Sys. Rev. Pharm.* **2018**, *9*, 70-78.
21. Daniel, P.; Supe, U.; Roymon, M.G. A review on phytochemical analysis of *Momordica charantia*. *Int. J. Adv. Pharm. Biol. Chem.* **2014**, *3*, 214-220.
22. Li, Y.-M.; Jia, M.; Li, H.-Q.; Zhang, N.-D.; Wen, X.; Rahman, K.; Zhang, Q.-Y.; Qin, L.-P. *Cnidium monnieri*: A Review of Traditional Uses, Phytochemical and Ethnopharmacological Properties. *Am. J. Chin. Med.* **2015**, *43*, 835-877, <https://doi.org/10.1142/S0192415X15500500>.
23. Bodun, D.S.; Abdulwahab, A.A.; Adegbenro, T.I.; Chidinma, E.O.; Osunnaya, S.A.' Alonge, M.O.; Diyaolu, Z.O.; Abdulazeez, M.T.; Abolade, R.O. Machine Learning-Based Drug Repositioning of Novel Human Aromatase Inhibitors Utilizing Molecular Docking and Molecular Dynamic Simulation. *Journal of Computational Biophysics and Chemistry*, **2025**, *24(3)*, .371-387.
24. Olugbogi, E.A.; Arobadade, O.A.; Bodun, D.S.; Omoseeye, S.D.; Omirin, E.S.; Fapohunda, O.; Ekun, O.E.; Metibemu, D.S.; Shodehinde, S.A.; Saliu, J.A.; Omotuyi, O.I. Identification of apposite antagonist for androgen receptor in prostate cancer: an in silico study of fenugreek compounds. *J. Biomol. Struct. Dyn.* **2024**, *42*, 12918-12934, <https://doi.org/10.1080/07391102.2023.2273988>.
25. Tao, X.; Huang, Y.; Wang, C.; Chen, F.; Yang, L.; Ling, L.; Che, Z.; Chen, X. Recent developments in molecular docking technology applied in food science: a review. *Int. J. Food Sci. Technol.* **2020**, *55*, 33-45, <https://doi.org/10.1111/ijfs.14325>.
26. Aribigbola, T.C.; Omoboyowa, D.A.; Bodun, D.S. Computational prediction of 11 $\beta$ -hydroxysteroid dehydrogenase inhibitors from n-butanol fraction of *Blighia welwetschii* (Hiern) leaf for the management of type-2 diabetes. *J. Biomol. Struct. Dyn.* **2024**, *42*, 10272-10285, <https://doi.org/10.1080/07391102.2023.2256869>.
27. Omoboyowa, D.A.; Bodun, D.S.; Saliu, J.A. Structure-based *in silico* investigation of antagonists of human ribonucleotide reductase from *Annona muricata*. *Inform. Med. Unlocked* **2023**, *38*, 101225, <https://doi.org/10.1016/j.imu.2023.101225>.
28. Ilesanmi, A.; Dairo, G.; Salimat, S.; Bodun, D.S.; Awoyale, B.; Balogun, T.A. Identification of bioactive compounds from *Vaccinium vitis-idaea* L. (Lingonberry) as inhibitors for treating KRAS-associated cancer: a computational approach. *In Silico Pharmacol.* **2023**, *11*, 32, <https://doi.org/10.1007/s40203-023-00165-1>.
29. Omoboyowa, D.A.; Kareem, J.A.; Saibu, O.A.; Bodun, D.S.; Ajayi, T.M.; Oyenyin, O.E. Identification of Phyto-Compounds from *Ilex kudingcha* as Inhibitors of Sterol-14 $\alpha$ -Demethylase Protease: A Computational Approach Against Chagas Disease. *Chem. Afr.* **2023**, *6*, 1335-1347, <https://doi.org/10.1007/s42250-022-00565-4>.
30. Luo, J.; Xue, Z.Q.; Liu, W.M.; Wu, J.L.; Yang, Z.Q. Koopmans' Theorem for Large Molecular Systems within Density Functional Theory. *J. Phys. Chem. A* **2006**, *110*, 12005-12009, <https://doi.org/10.1021/jp063669m>.
31. Parr, R.G.; Pearson, R.G. Absolute hardness: companion parameter to absolute electronegativity. *Journal of the American chemical society.* **1983**, *105*, 7512-7516, <https://doi.org/10.1021/ja00364a005>.
32. Lipinski, C.A. Lead- and drug-like compounds: the rule-of-five revolution. *Drug Discov. Today Technol.* **2004**, *1*, 337-341, <https://doi.org/10.1016/j.ddtec.2004.11.007>.
33. Baell, J.B.; Holloway, G.A. New Substructure Filters for Removal of Pan Assay Interference Compounds (PAINS) from Screening Libraries and for Their Exclusion in Bioassays. *J. Med. Chem.* **2010**, *53*, 2719-2740, <https://doi.org/10.1021/jm901137j>.
34. Santos, J.L.D. Pan-Assay Interference Compounds (PAINS): Warning Signs in Biochemical-Pharmacological Evaluations. *Biochem. Pharmacol.* **2015**, *4*, 1000e173, <http://dx.doi.org/10.4172/2167-0501.1000e173>.
35. Olugbogi, E.A.; Bodun, D.S.; Omoseeye, S.D.; Onoriode, A.O.; Oluwamroti, F.O.; Adedara, J.F.; Oriyomi, I.A.; Bello, F.O.; Olowoyeye, F.O.; Laoye, O.G.; Adebowale, D.B.; Adebisi, A.D.; Omotuyi, O.I. *Quassia amara* bioactive compounds as a Novel DPP-IV inhibitor: an in-silico study. *Bull. Natl. Res. Cent.* **2022**, *46*, 217, <https://doi.org/10.1186/s42269-022-00890-1>.
36. Sherman, W.; Beard, H.S.; Farid, R. Use of an Induced Fit Receptor Structure in Virtual Screening. *Chem. Biol. Drug Des.* **2006**, *67*, 83-84, <https://doi.org/10.1111/j.1747-0285.2005.00327.x>.
37. Tripathi, S.K.; Selvaraj, C.; Singh, S.K.; Reddy, K.K. Molecular docking, QPLD, and ADME prediction studies on HIV-1 integrase leads. *Med. Chem. Res.* **2012**, *21*, 4239-4251, <https://doi.org/10.1007/s00044-011-9940-6>.

38. Elekofehinti, O.O.; Iwaloye, O.; Olawale, F.; Chukwuemeka, P.O.; Folorunso, I.M. Newly designed compounds from scaffolds of known actives as inhibitors of survivin: computational analysis from the perspective of fragment-based drug design. *In Silico Pharmacol.* **2021**, *9*, 47, <https://doi.org/10.1007/s40203-021-00108-8>.
39. Kaavin, K.; Naresh, D.; Yogeshkumar, M.R.; Krishna Prakash, M.; Janarthan, S.; Murali Krishnan, M.; Malathi, M. *In-silico* DFT studies and molecular docking evaluation of benzimidazo methoxy quinoline-2-one ligand and its Co, Ni, Cu and Zn complexes as potential inhibitors of Bcl-2, Caspase-3, EGFR, mTOR, and PI3K, cancer-causing proteins. *Chem. Phys. Impact* **2024**, *8*, 100418, <https://doi.org/10.1016/j.chphi.2023.100418>.
40. de Oliveira, M.T.; and Katekawa, E. On the Virtues of Automated Quantitative Structure–Activity Relationship: The New Kid on the Block. *Future Med. Chem.* **2018**, *10*, 335-342, <https://doi.org/10.4155/fmc-2017-0170>.
41. Wang, S.; Shen, J.; Zhang, B.; Tian, J.; Zhao, W.; Wu, W. Molecular mechanism study of cancer treatment based on network pharmacology of lily. *Highl. Sci. Eng. Technol.* **2022**, *14*, 397-403, <https://doi.org/10.54097/hset.v14i.1852>.
42. Akinmoladun, A.C.; Adetuyi, A.R.; Komolafe, K.; Oguntibeju, O.O. Nutritional benefits, phytochemical constituents, ethnomedicinal uses and biological properties of Miracle fruit plant (*Synsepalum dulcificum* Shumach. & Thonn. Daniell). *Heliyon* **2020**, *6*, e05837, <https://doi.org/10.1016/j.heliyon.2020.e05837>.
43. Lee, J.; Kim, J.H. Kaempferol Inhibits Pancreatic Cancer Cell Growth and Migration through the Blockade of EGFR-Related Pathway *In Vitro*. *PloS ONE*, **2016**, *11*, e0155264, <https://doi.org/10.1371/journal.pone.0155264>.

## Publisher's Note & Disclaimer

The statements, opinions, and data presented in this publication are solely those of the individual author(s) and contributor(s) and do not necessarily reflect the views of the publisher and/or the editor(s). The publisher and/or the editor(s) disclaim any responsibility for the accuracy, completeness, or reliability of the content. Neither the publisher nor the editor(s) assume any legal liability for any errors, omissions, or consequences arising from the use of the information presented in this publication. Furthermore, the publisher and/or the editor(s) disclaim any liability for any injury, damage, or loss to persons or property that may result from the use of any ideas, methods, instructions, or products mentioned in the content. Readers are encouraged to independently verify any information before relying on it, and the publisher assumes no responsibility for any consequences arising from the use of materials contained in this publication.